2023-07

Astronomically forced saline lake deposition and paleoclimatic response in the Huanggang Basin during the Paleogene, Eastern China

Song, C

10.1016/j.oregeorev.2023.105506
Ore Geology Reviews
Elsevier BV

Ore Geology Reviews 158 (2023) 105506

Contents lists available at ScienceDirect

Ore Geology Reviews

journal homepage: www.elsevier.com/locate/oregeorev

Astronomically forced saline lake deposition and paleoclimatic response in the Huanggang Basin during the Paleogene, Eastern China

Cuiyu Song [a], Dawei Lv [a,b,*], Jie Chang [c,*], John I. Ejembi [d], Lulu Tang [c], Munira Raji [e], Wentao Chen [a,c], Zhihui Zhang [a]

[a] College of Earth Science and Engineering, Shandong University of Science and Technology, Qingdao 266590, China
[b] Laboratory for Marine Mineral Resources, Qingdao National Laboratory for Marine Science and Technology, Qingdao 266071, China
[c] Shandong Institute of Geological Sciences, Ji'nan 250013, China
[d] JiE Ventures, Houston, TX 77449, USA
[e] Sustainable Earth Institute (SEI), University of Plymouth, Drake Circle, Plymouth PL48AA, UK

ARTICLE INFO

Keywords:
Halite
Paleoclimate
Astronomical forcing
Short orbital eccentricity
Huanggang Basin
Paleogene

ABSTRACT

Halite is a type of evaporite that can be processed into refined salt for food processing, and used as an important raw material in the chemical industry. However, our understanding of the astronomical forcing pattern on halite formation at the sedimentary basin scale is still limited. Here, we present a halite-rich lacustrine record from the middle-late Eocene through the early Oligocene of the Dawenkou Formation in the Huanggang Basin, Eastern China. A ~ 6.5-Myr-long floating astronomical time scale was constructed based on a 405-kyr orbital eccentricity cycle tuning of gamma-ray (GR) series measured from the Upper and Middle members of the Dawenkou Formation. Our results indicate that halite intervals in the Middle Member of the Dawenkou Formation correspond well with the minima of the 100 kyr orbital eccentricity, suggesting the short eccentricity-induced climatic cycles forcing of halite formation by impact on seasonal contrasts. Our work provides essential context for understanding the pattern of halite deposits from the aspect of climate cycles at the sedimentary basin scale.

1. Introduction

Evaporites are rocks composed of chemically precipitated minerals derived from naturally occurring brines that result from saturated concentration either by evaporation or freeze-drying (Sonnenfeld, 1984). Bays, lagoons, and dry areas on continents are all favorable environments for evaporite formation (e.g., Liu et al., 1987; Williams, 1991; Worley, 2005; Huang and Hinnov, 2014). Halite is a type of evaporite that can be processed into refined salt for a variety of use cases, e.g., for food processing, and it is also an important raw material in the chemical industry, such as the production of alkali, hydrochloric acid, chlorine, sodium metal, etc (Sonnenfeld, 1984).

Salt deposits are formed from the evaporation of saline water in salt-bearing basins. An arid/semi-arid climate, coupled with evaporation exceeding the water replenished rate in the basin, are fundamental conditions for saline deposition (Smykatz-Kloss and Roy, 2010; Filippi et al., 2011; Li et al., 2020a). Over geologic timescales, climatic conditions have repeatedly changed between wet and dry, forming climate cycles (Anderson, 2011; Hinnov, 2013; Lv et al., 2022; Wang et al., 2022). The variation in insolation, which is induced by the quasi-periodic variations in the Earth's orbital eccentricity, obliquity, and precession index (also known as Milankovitch cycles), has been proven to be key drivers of climate change at 10^4-to-10^6-year time scales (Hinnov, 2013; Zhang et al., 2015; Li et al., 2016a; Sinnesael et al., 2021; Lepre and Quinn, 2022; Wu et al., 2022). The Milankovitch cycles as identified in the sedimentary record can help to establish high-precision chronological frameworks (Wu et al., 2013; Eldrett et al., 2015a; Liu et al., 2018; Boulila et al., 2018; Zhang et al., 2020b), to enhance the understanding of some geological events, such as the occurrence of the oceanic anoxic event (Kemp et al., 2011; Li et al., 2020b), the late Devonian mass extinction event (De Vleeschouwer et al., 2017) and wildfire activity (Zhang et al., 2020c; Hollaar et al., 2021; Zhang et al., 2022), and sedimentary systems in general (Eldrett et al., 2015b; Yao et al., 2015; Li and Barnes, 2019; Zhang et al., 2020a).

Several studies have documented astronomical forcings that led to the formation of evaporites (e.g., Williams, 1991; Xiao et al., 2010; Abels et al., 2011; Huang and Hinnov, 2019). In the late Ordovician-early Silurian marginal marine bedded halite deposits and the Eocene

* Corresponding authors at: College of Earth Science and Engineering, Shandong University of Science and Technology, Qingdao 266590, China (D. Lv).
E-mail addresses: lvdawei95@sdust.edu.cn (D. Lv), changjiedky@shandong.cn (J. Chang).

https://doi.org/10.1016/j.oregeorev.2023.105506
Received 30 December 2022; Received in revised form 22 May 2023; Accepted 23 May 2023
Available online 1 June 2023

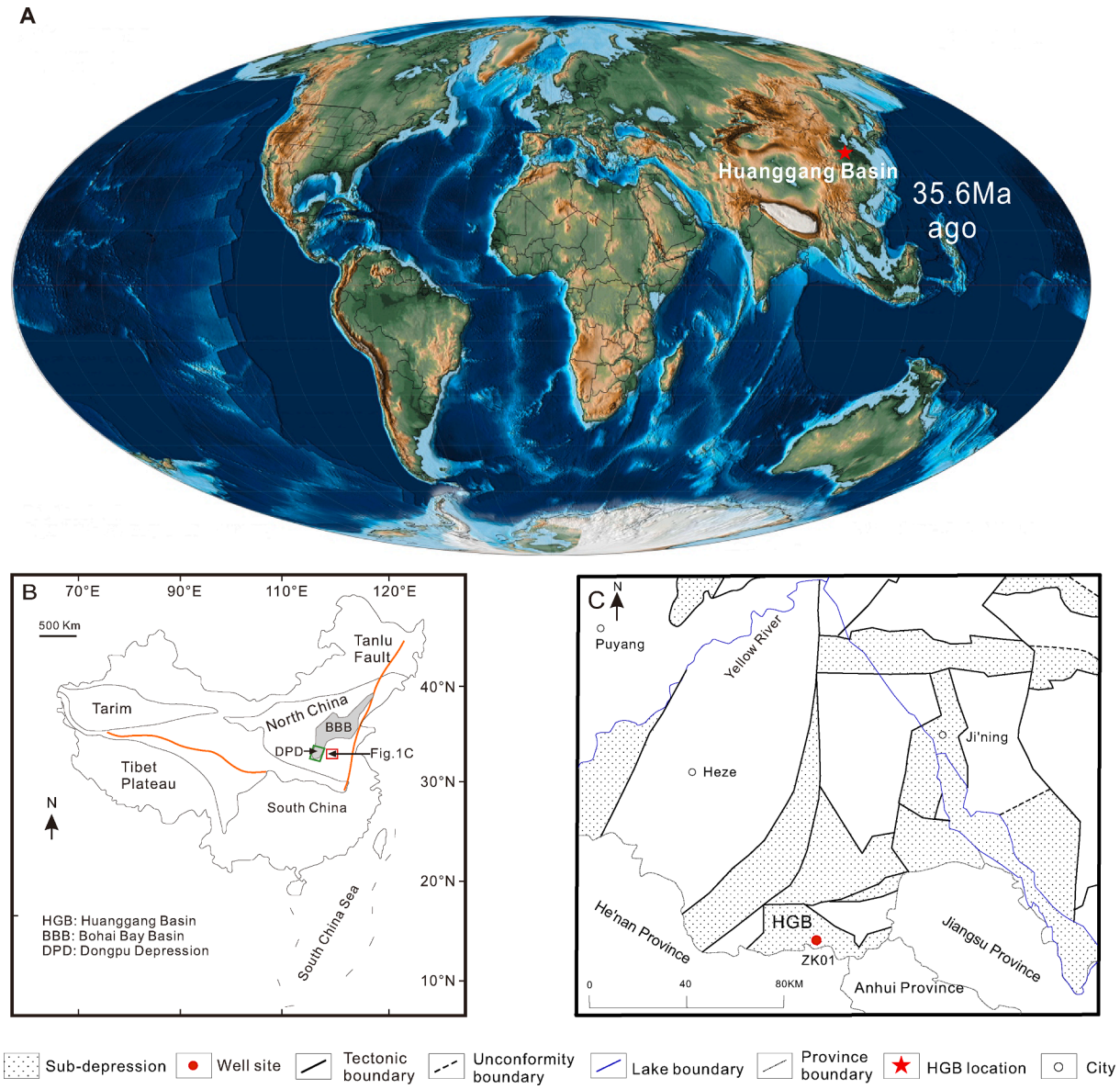

Fig. 1. Geologic setting of the Huanggang Basin, China. (A) Paleogeographic map of the continents during the Oligocene (35.6 Ma ago) showing the location of the Huanggang Basin (Scotese and Wright, 2018). (B) Map showing local tectonic features within the vicinity of the Huanggang Basin: the Tanlu Fault, the Bohai Bay Basin (BBB), and the Dongpu Depression (DPD). (C) Regional tectonic map of the Huanggang Basin and adjacent localities (modified from Tang et al., 2021).

terrestrial basins, salt-bearing depositions were found to be paced by ~ 100-kyr orbital eccentricity cycles (e.g., Williams, 1991; Abels et al., 2011; Huang and Hinnov, 2019). However, 41-kyr obliquity was deemed to be the dominant forcing of gypsum deposition during ~ 35 Ma to 33 Ma in the Xining Basin (Xiao et al., 2010).

During the Paleogene Period, massive halite deposits were formed in the southwestern Shandong Province in eastern China (Liu et al., 1987). For example, the Huanggang Basin contain a super-large halite deposit with an estimated reserve of over 20 billion tons (Tang et al., 2021). However, owing to the rare occurrence of magmatic rocks and paleontological remains of the salt-bearing strata, the chronological research about this record is extremely limited. The currently accepted salt-forming age of this strata is approximately from the middle and late Eocene to the Oligocene (Liu et al., 1987; Lu et al., 2021). The high-precision chronological framework has not yet been constructed for this saline lacustrine record, and the forcing of astronomical orbit on the halite formation remains unknown.

In this study, we present a continental paleoclimatic record from the middle and late Eocene through the early Oligocene of the Dawenkou Formation in the Huanggang Basin, China (Fig. 1). This lacustrine sequence illustrates a more than 600 m-thick succession with decimeter to decameter-scale halite-gypsum mudstone-mudstone rhythms in the Middle Member of the Dawenkou Formation, representing the responses to the orbitally forced climate change and lake level variations in the Huanggang Basin. We constructed the floating astronomical time scale (FATS) by tuning this rhythmic succession to the 405-kyr orbital eccentricity cycles and proposed a conceptual model to explore the influence of climate change and control of short eccentricity on halite formation.

2. Geological setting

The Huanggang Basin is located south of the Shanxian city in the southwest of Shandong Province, North China (34.5°N, 116°E; Fig. 1). It is a fault basin that formed in the late Cretaceous from the effect of the Tanlu strike-slip fault system in eastern China. In terms of the geotectonic location, the Huanggang sub-depression is about 150 km to the east of the Dongpu Depression of the Bohai Bay Basin (Fig. 1B), trending

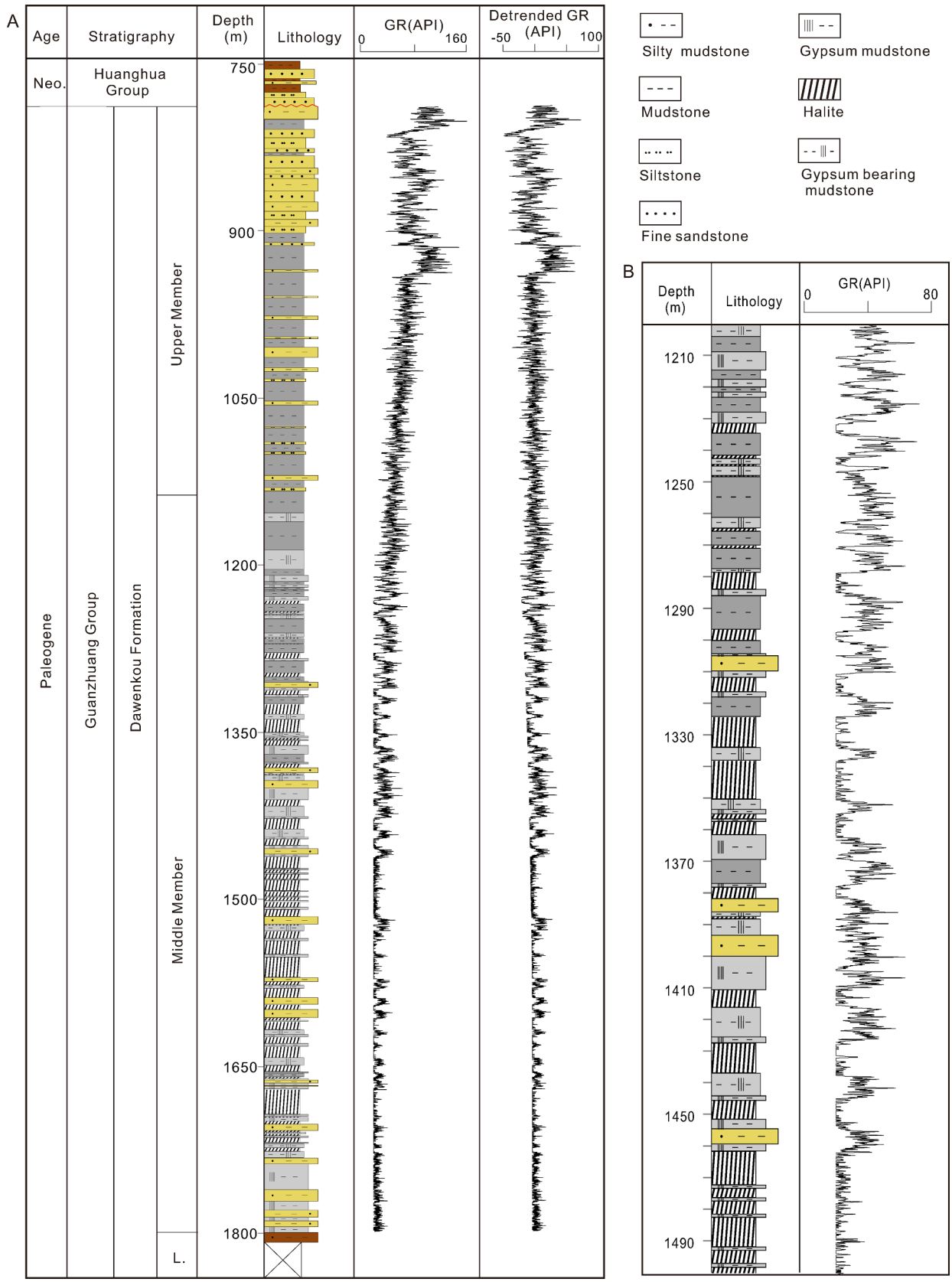

Fig. 2. Stratigraphic section and gamma-ray (GR) logs of (A) the Upper and Middle members of the Dawenkou Formation in the Huanggang Basin, and (B) the magnified portion for depth 1200–1500 m.

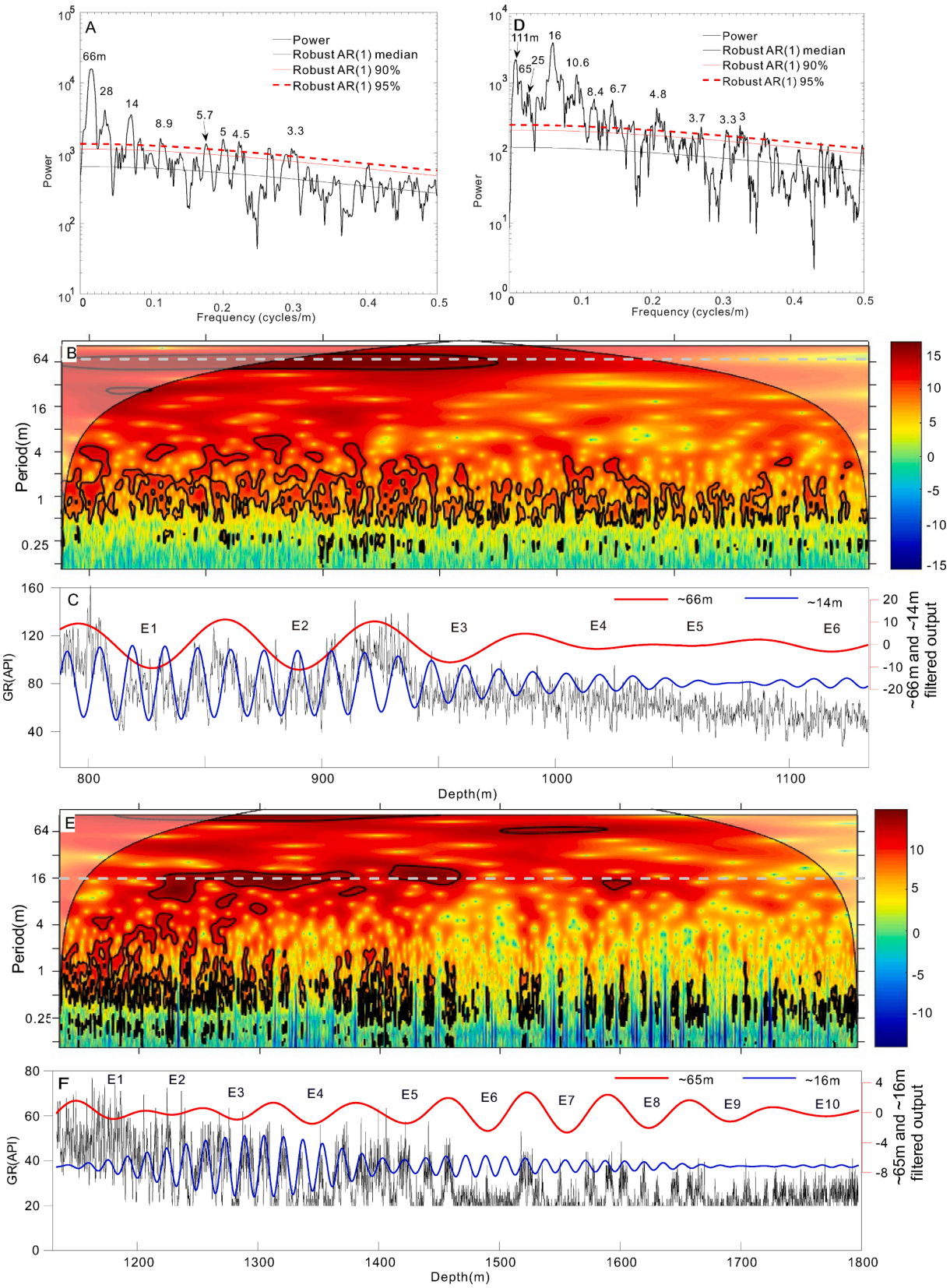

Fig. 3. The MTM spectrum, wavelet spectrum, and band-pass filtering of the Upper (A–C) and Middle (D–F) members of the Dawenkou Formation. (A) and (D) are the 2π MTM power spectrum of the GR series. (B) and (E) are the wavelet spectrum of the GR series. The black contour lines in (B) and (E) enclose an area with more than 95% confidence level, and white dashed lines indicate ~66 m cycles and ~16 m cycles, respectively. (C) and (F) are GR series with ~66 m, ~14 m, ~65 m, and ~16 m filtered output curves (passband: 0.0151 ± 0.003, 0.0714 ± 0.005, 0.0154 ± 0.003, and 0.0625 ± 0.003).

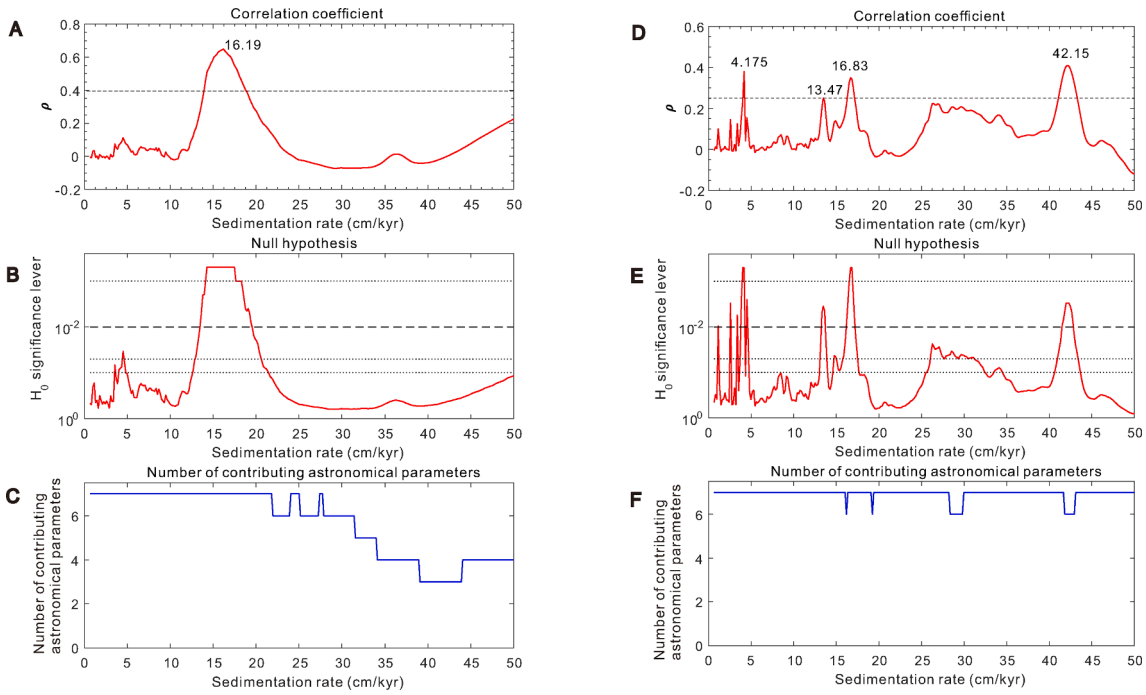

Fig. 4. The correlation coefficient (COCO) analysis of the Middle and Upper members of the Dawenkou Formation. (A) and (D) are COCO analyses with labeled potential sedimentation rates.(B) and (E) are null hypotheses (H0, no astronomical forcing). The tests show 14.27–18.27 cm/kyr sedimentation rate have H0 significance levels less than 0.001 for GR series (788.25–1133.45 m for the Upper Member) in (B) and ~4.18, 13.47, 16.83, and 42.15 cm/kyr sedimentation rate with less than 0. 01 H0 significance levels for GR series (1133.45–1797.30 m for the Middle Member) in (E). (C) and (F) are the number of contributing astronomical parameters in tested sedimentation rate, and the target series for both (C) and (F) is the La2004 astronomical solution at 35 Ma. The significance levels are estimated using a Monte Carlo simulation of 2000 iterations with a step of 0.16 cm/kyr.

toward east of the North China plate.

During the Paleogene, a continuous and widespread shallow and saline lacustrine succession rich in halite, gypsum, and other salt minerals developed in the Dawenkou Formation, Guanzhuang Group of the Huanggang Basin. The Dawenkou Formation can be divided into three members (Tang et al., 2021). The Lower Member is mainly brownish-red to purplish-red mudstone and argillaceous siltstone, reflecting shallow lacustrine sedimentation under oxidizing conditions. The Middle Member is the salt-bearing succession containing grayish-white gypsum mudstone/halite interbedded with dark-gray mudstone/silty mudstone, with the thickness of the halite intervals ranging from 0.3 m to 22.95 m. The lithology of the upper section consists mainly of gray/grayish green mudstone, yellow/light yellow silty mudstone and siltstone with occasional gravel beds at the bottom, reflecting shallow to semi-deep lacustrine sedimentation under reducing conditions. The Guanzhuang Group is in unconformable contact with the overlying Neogene Huanghua Group.

The depositional age of the Dawenkou Formation in the Huanggang Basin has not been determined using high precision techniques. A previous study places the salt-forming age in southwestern Shandong in the middle-late Eocene to Oligocene (Liu et al., 1987).

3. Data and methods

3.1. Gamma-ray well log data

The gamma-ray (GR) well log data in this study is from the ZK01 borehole in the Huanggang Basin depocenter (location of the borehole is in Fig. 1C). The data covers the Middle to Upper members of the Dawenkou Formation from approximately 788.25 m to 1797.30 m with a spacing of 0.05 m. The GR well logs capture variations in naturally occurring radiation from potassium (K), thorium (Th), and uranium (U) in sands, shales, and clays. Since halite contains low amounts of K, Th, and U, salt-rich intervals have low GR values, while mudstone-rich intervals have relatively high GR values. During halite intervals with dominantly low GR values, occasionally elevated values appear which might be due to the occurrence of small amount of potassium salts (Fig. 2B in detail).

3.2. Time series analysis

We performed the multitaper method (MTM) spectral analysis with robust red noise modeling on the untuned and tuned GR log spectrum after the detrended processing. Also, the Gaussian band-pass filtering was applied to isolate orbital cycles in the series. We utilized the Taner filter and the Hilbert transform to generate the amplitude modulation of the short eccentricity period, and the evolutionary wavelet spectra were conducted to track the change of frequency with depth. We used the correlation coefficient method (COCO) to evaluate the most probable sedimentation rate for a sedimentary sequence, given a specific astronomical forcing target (Li et al., 2018). Time scale optimization (TimeOpt) method (Meyers, 2015) was also employed to estimate the optimal sedimentation rate by simultaneously optimizing the precession-eccentricity variances and eccentricity-related amplitude modulation of the precession frequency band (Meyers, 2015). Astronomical tuning was carried out to construct the floating astronomical time scale (FATS) by fixing the duration of cycles isolated through filtering. All the functions mentioned above were implemented in Acycle V 2.4 (Li et al., 2019).

4. Results

In general, the GR records show different characteristics between 788.25 and 1133.45 m of the Upper Member, and 1133.45–1797.30 m of the Middle Member of the Dawenkou Formation (Fig. 2). The sedimentary strata of the Middle Member record mainly low GR values (~20 API, corresponding to halites) but interrupted by several high GR intervals (~80 API). The Upper Member sedimentary strata record

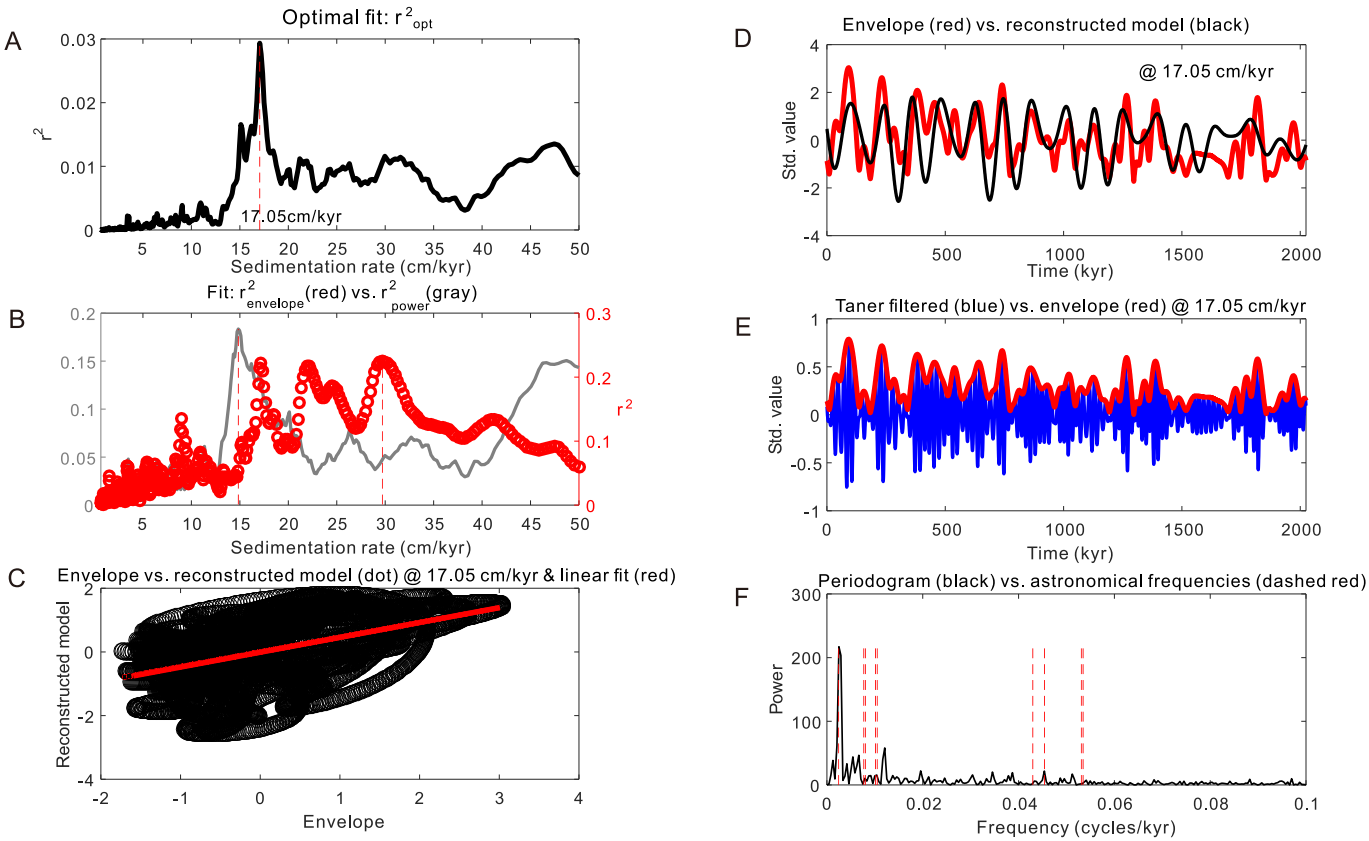

Fig. 5. TimeOpt generated sedimentation rate for the Upper Member of the Dawenkou Formation. (A) Combined envelope and spectral power fit (r^2opt) at test deposition rate. (B) Squared correlation coefficient for the amplitude envelope fit (r^2envelope, red dot) and the spectral power fit (r^2power, gray). (C) Correlation of the envelope of filtered precession signals and reconstructed eccentricity model. (D) Envelope of filtered precession signals (red) and reconstructed eccentricity model (black) at sedimentation rate of 17.05 cm/kyr. (E) Taner filtered time series using a sedimentation rate of 17.05 cm/kyr (blue) and its envelope (red). (F) Periodogram of the gamma-ray time series using a sedimentation rate of 17.05 cm/kyr and input astronomical frequencies. Here 500 test sedimentation rates range from 0.659 to 50 cm/kyr. The eccentricity and precession cycles in La2004 solution at ~ 35 Ma are 409.60 kyr, 132.13kyr, 124.12 kyr, 99.90 kyr, 95.26 kyr, 23.27 kyr, 22.02 kyr, 18.88 kyr, and 18.70 kyr. We used 2000 Monte Carlo simulations to evaluate the significance level of the r^2 values. Taner bandpass cut-off frequencies are 0.0355 and 0.0659 cycles/kyr with a roll-off rate of 10^{12}.

relatively high GR values. The MTM power spectral analysis, evolutionary wavelet spectra, COCO anaysis, and timeOpt analysis were separately carried out on linearly detrended records of the Upper and Middle members of the Dawenkou Formation.

4.1. GR series of the Upper Member of the Dawenkou Formation

The Upper Member of the Dawenkou Formation (788.25–1133.45 m) covers a thickness of 345.20 m (Fig. 2). The MTM power spectrum of the untuned GR profile shows significant peaks (greater than 95% confidence level) at wavelengths of 66.0, 28.0, 14.0, 8.9, 5.7, 5.0, 4.5 and 3.3 m. The ratios of 66.0 m, 14.0 m, 5.7 m, and 3.3 m are close to those of 405 kyr, 100 kyr, 40 kyr, and 20 kyr thus indicating the preservation of Milankovitch frequencies in the record (Fig. 3A). The evolutionary wavelet power spectrum of the GR log series in the depth domain indicates dominant ~ 66 m (greater than 95% confidence level) cycling through ~ 850–975 m in the Upper Member of the Dawenkou Formation (Fig. 3B).

In the COCO analysis, the tested sedimentation rates were set from 0.65 to 50 cm/kyr, and the target series is the La2004 astronomical solution at 35 Ma. A single dominant peak at 16.19 cm/kyr is present in the COCO plot, with the correlation coefficient higher than 0.6 and the null hypothesis significance levels lower than 0.001 (i.e., representing the calculated probability of no orbital forcing in the record; Fig. 4) thus implying the optimal sedimentation rate for the Upper Member of the Dawenkou Formation.

TimeOpt analysis result supports that the optimal sedimentation rate is 17.05 cm/kyr with the highest r^2opt value (Fig. 5A). The null hypothesis analysis of the r^2envelope, r^2power, and r^2opt values indicates the significance level of 4.6%, 6.3% and 1.1% respectively (Fig. 6), implying the mean sedimentation rate of the GR series for the Upper Member of the Dawenkou Formation should be 17.05 cm/kyr, similar to the COCO analysis result.

Previous studies of the adjacent basins (e.g., the Dongying and Jianghan basins) in the Paleogene show that the sedimentary rate of lacustrine siltstone-mudstone rhythm usually ranges from 5.7 to 30 cm/kyr (Liu et al., 2018; Shi et al., 2018; Huang and Hinnov, 2019; Shi et al., 2019; Shi et al., 2020; Du et al., 2020; Wang et al., 2020; and Shi et al., 2021), which is consistent with the estimated optimal sedimentation rate in our study. In accordance with the estimated sedimentation rate of 16.19 cm/kyr, the 66.0 m cycles represent 408 kyr cycles, the 14.0 m cycles correspond to 86 kyr cycles, the 5.7 m and 3.3 m cycles correspond to 35 kyr and 20 kyr cycles, respectively. Thus, the ~66.0 m and ~14.0 m cycles are interpreted as ~405 kyr and 100 kyr orbital eccentricity cycles. We bandpass-filtered the ~66.0 m and ~14.0 m cycles for the GR series in the depth domain using a Gaussian band-pass filter and recognized five to six ~66.0 m cycles, indicating that the sedimentation of the Upper Member of the Dawenkou Formation lasted from 2.025 – 2.43 Myr (Fig. 3C).

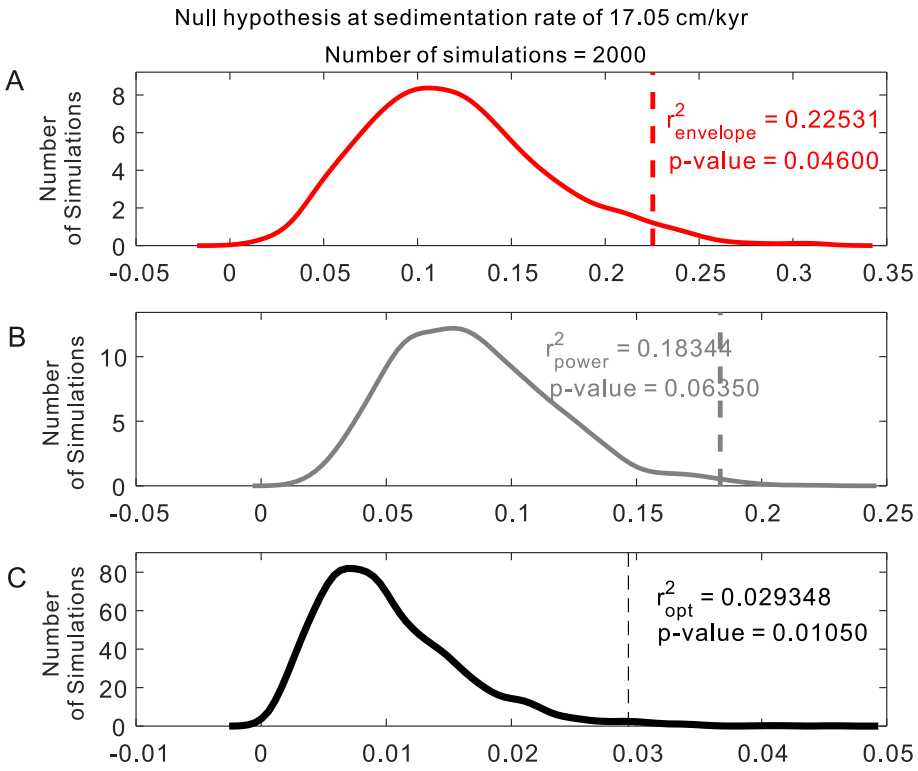

Fig. 6. Summary of 2000 Monte Carlo simulations with AR (1) surrogates used to evaluate the significance levels of the maximum observed r^2envelope (A), r^2power (B), and r^2opt (C) for the Upper Member of the Dawenkou Formation.

4.2. GR series of the Middle Member of the Dawenkou Formation

The Middle Member of the Dawenkou Formation is the salt-bearing strata with a thickness of 663.85 m (from 1133.45 m to 1797.30 m). The MTM power spectrum of the GR profile shows significant peaks (>95% confidence level) at wavelengths of 111.0, 65.0, 25.0, 16.0, 10.6, 8.4, 6.7, 4.8, 3.7, 3.3, and 3.0 m. The ratios of ~ 65.0 m, 16.0 m, 6.7 m, and 3.3 m, along with ratios of ~ 111.0 m, 25.0 m, 10.6 m, and 4.8 m are both close to those of 405 kyr, 100 kyr, 40 kyr, and 20 kyr thus implying the preservation of Milankovitch frequencies in the studied strata (Fig. 3D). The evolutionary wavelet power spectrum of the GR series in the depth domain shows strong ~ 16 m (>95% confidence level) cycling through 1200–1460 m in the Middle Member of the Dawenkou Formation (Fig. 3E).

The sedimentation rate of evaporite is mainly influenced by provenance and sedimentary environment. The implied net rate of deposition of the Mallowa Salt in the Canning Basin of Western Australia is 113 cm/kyr for the halite succession deposited in a barred marginal-marine to ephemeral saltpan and saline mudflat environments during the late Ordovician to early Silurian, which is of the same order as those estimated for other thick evaporite sequences of Palaeozoic age (Williams, 1991). The estimated sedimentation rates of lacustrine salt-bearing strata in the Jianghan Basin of Central China in the Eocene and Oligocene are 14.8–30.0 cm/kyr and 5.7–11.6 cm/kyr, respectively (Huang and Hinnov, 2019). However, the sedimentation rate of mudstone-gypsum cycles in the Xining Basin at the northeastern edge of the Tibetan Plateau is just 2.1–4.8 cm/kyr (Abels et al., 2011). Generally, the sedimentation rate of halite might be relatively high while the muddy materials seem to be deposited more slowly, leading to a reduced average accumulation rate for the mudstone-halite cycles. In view of the similarity between the salt-bearing strata in the Jianghan and Huanggang basins in terms of the depositional age and environment, the sedimentation rate of the Huanggang Basin might be closer to that of the Jianghan Basin.

To find the optimal sedimentation rate for the studied interval, a COCO analysis with 2000 Monte Carlo simulations was performed on tested sedimentation rates ranging from 0.65 to 50 cm/kyr. Several peaks at ~ 4.18 cm/kyr, 13.47 cm/kyr, 16.83 cm/kyr, and 42.15 cm/kyr are present in the COCO analysis (Fig. 4D). Amongst these peaks, 13.47 cm/kyr and 16.83 cm/kyr values are within the range of sedimentation rate for the halite-mudstone rhythm in the Jianghan Basin, implying the probable sedimentation rates for these strata. Both sedimentation rates have null hypothesis significance levels lower than 0.01. For the above MTM analysis results, if the combination of ~ 111.0 m, 25.0 m, 10.6 m, and 4.8 m corresponded to Milankovitch cycles, the ~ 111.0 m cycle could not be interpreted as 405 kyr cycle either with the sedimentation rate of 13.47 cm/kyr or 16.83 cm/kyr. Therefore, it is more reasonable for the combination of ~ 65.0 m, 16.0 m, 6.7 m, and 3.3 m to be interpreted as Milankovitch cycles. Furthermore, if the sedimentation rate is 13.47 cm/kyr, the 65.0 m cycles represent 483 kyr cycles, the 16.0 m cycles correspond to 119 kyr cycles, and the 6.7 m and 3.3 m cycles correspond to 50 kyr and 24 kyr cycles, respectively. If the sedimentation rate is 16.83 cm/kyr, the 65.0 m cycles represent 386 kyr cycles, the 16.0 m cycles correspond to 95 kyr cycles, the 6.7 m and 3.3 m cycles correspond to 40 kyr and 20 kyr cycles, respectively. Considering the correlation coefficient and margin of error, the 16.83 cm/kyr is the most likely average deposition rate for the salt-bearing strata.

TimeOpt analysis suggests that the optimal sedimentation rate is 16.71 cm/kyr with the highest r^2opt value (Fig. 7A). In comparison, there are two other peaks in the r^2opt plot at 26.65 cm/kyr and 29.15 cm/kyr. However, the null hypothesis analysis of these r^2 values shows that only the r^2opt at the sedimentation rate of 16.71 cm/kyr has a significance level of ~ 5% (Fig. 8). In contrast, the significance level of the r^2opt at 26.65 cm/kyr and 29.15 cm/kyr are higher than 50% (Fig. 9). Taken together, it is more reasonable that the mean sedimentation rate for the Middle Member of the Dawenkou Formation is 16.71 cm/kyr, which is consistent with that from the COCO analysis (16.83 cm/kyr).

Band-pass filtering of the ~65.0 m and ~16.0 m cycles for the GR series in the depth domain was conducted and about ten ~65.0 m cycles

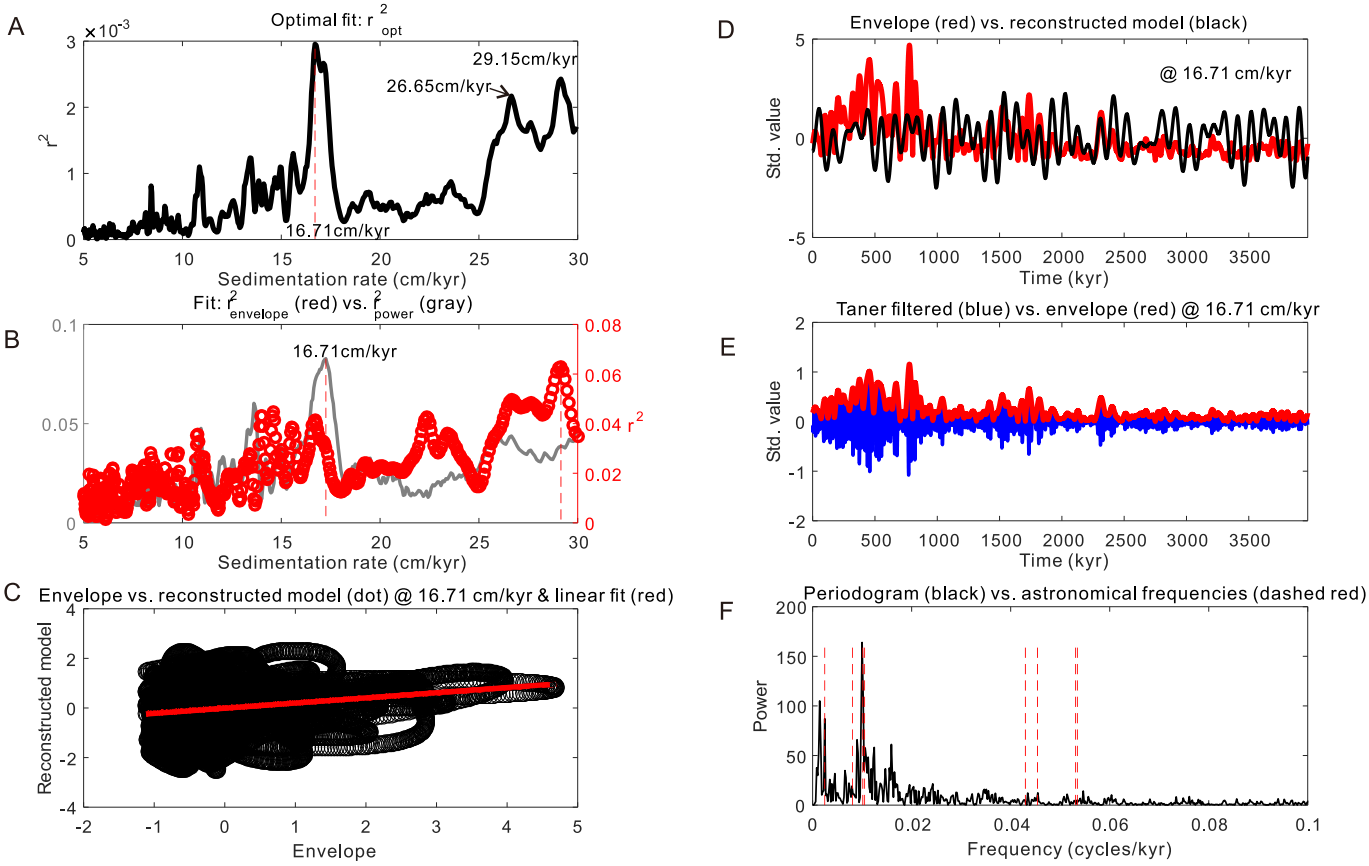

Fig. 7. TimeOpt generated sedimentation rate for the Middle Member of the Dawenkou Formation. (A) Combined envelope and spectral power fit (r^2opt) at test deposition rate. (B) Squared correlation coefficient for the amplitude envelope fit (r^2envelope, red dot) and the spectral power fit (r^2power, gray). (C) Correlation of the envelope of filtered precession signals and reconstructed eccentricity model. (D) Envelope of filtered precession signals (red) and reconstructed eccentricity model (black) at sedimentation rate of 16.71 cm/kyr. (E) Taner filtered time series using a sedimentation rate of 16.71 cm/kyr (blue) and its envelope (red). (F) Periodogram of the gamma-ray time series using a sedimentation rate of 16.71 cm/kyr and input astronomical frequencies. Here 500 test sedimentation rates range from 5 to 30 cm/kyr. The eccentricity and precession cycles in La2004 solution at ~ 35 Ma are 409.60 kyr, 124.12 kyr, 99.90 kyr, 95.26 kyr, 23.27 kyr, 22.02 kyr, 18.88 kyr, and 18.70 kyr. We used 2000 Monte Carlo simulations to evaluate the significance level of the r^2 values. Taner bandpass cut-off frequencies are 0.0355 and 0.0659 cycles/kyr with a roll-off rate of 10^{12}.

were recognized, suggesting that sedimentation of the Middle Member of the Dawenkou Formation lasted for nearly 4.05 Myr (Fig. 3F).

4.3. The combined 405-kyr-tuned GR time series for the Middle and Upper members of the Dawenkou Formation

We combined the Gaussian band-pass filtering of ~ 66 m and ~ 65 m cycles for the GR series of the Upper and Middle Dawenkou Formation (Fig. 10A) to generate the age model (Fig. 10C) according to the curve vertices. The whole GR data was then astronomically calibrated to establish the FATS of the studied interval. The results show that the sedimentation time of the Middle and Upper Dawenkou Formation spans about 6.5 Myr (Fig. 10B), with deposition rates ranging from 11 cm/kyr to 19 cm/kyr (Fig. 10A).

The constructed FATS of the Upper and Middle Dawenkou Formation has one main source of uncertainty, that is, the identified long eccentricity cycles in our FATS, which may lead to an uncertainty of one 405-kyr cycle (~0.4 Myr) (Wang et al., 2020). Accordingly, the duration of the Upper and Middle member of the Dawenkou Formation is 6.5 ± 0.4 Myr.

The MTM power spectrum of the 405-kyr-tuned GR series illustrates significant cycles of 405 kyr, 125kyr, 100 kyr, 62kyr, 44kyr, 40 kyr, 26kyr and 20 kyr (Fig. 10D).

5. Discussion

5.1. Chronological framework

Based on the pollen assemblage analysis from the Dawenkou Formation of the Dawenkou Basin near the Huanggang Basin, the Dawenkou Formation can be divided into two parts: The deposition period of the lower part occurred during the late Eocene to early Oligocene, which is contemporaneous with the fourth member of the Shahejie Formation (Es4) in the Bohai Bay Basin (BBB), whereas the upper part was deposited during the early Oligocene, equivalent to the third member of the Shahejie Formation (Es3) in the BBB (Lei, 1984). However, according to the latest chronological framework of the Shahejie Formation in the BBB, the above stratigraphic relationships are not consistent with the widely recognized salt-forming age of the Dawenkou Formation (i.e., from the middle-late Eocene to the early Oligocene).

Liu et al. (2018) established a high-precision chronological framework of the BBB at 66–23 Ma based on the K/Ar dating results, magnetostratigraphy, and the Oligocene/Miocene boundary age constraint (23.03 Ma) in GTS2012. The obtained duration of the fourth, third, second (Es2), and first (Es1) members of the Shahejie Formation were 50.80–42.47 Ma, 42.47–35.99 Ma, 35.99–31.94 Ma, and 31.94–28.86 Ma, respectively (Fig. 11). Therefore, the Middle and Upper members of the Dawenkou Formation deposited from the middle-late Eocene to Oligocene may be equivalent to the sedimentary ages of Es3 and Es2 in

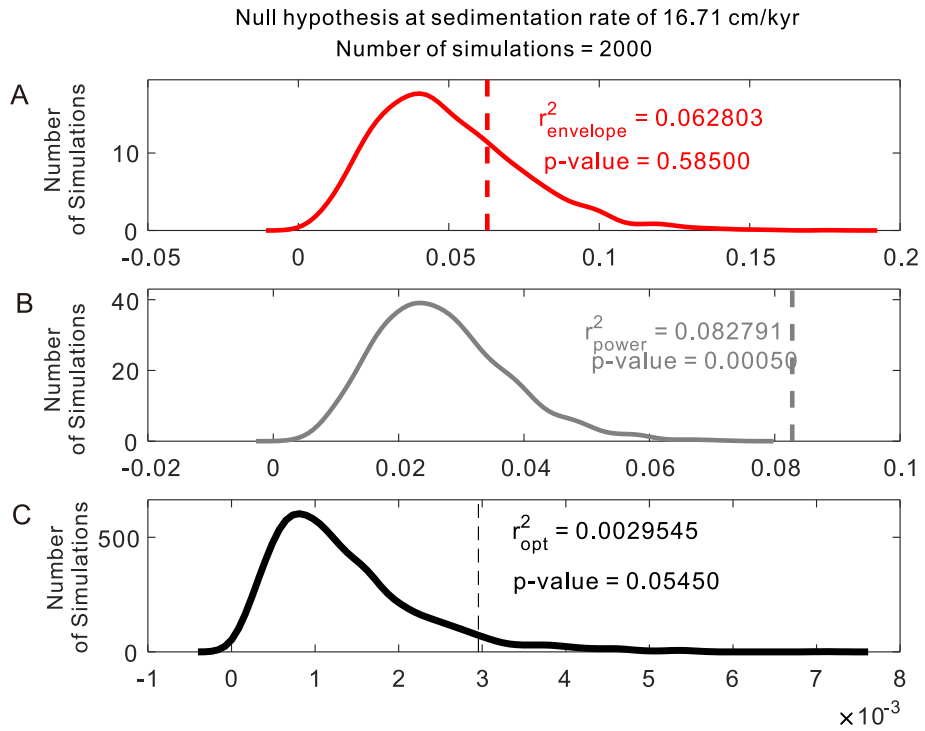

Fig. 8. Summary of 2000 Monte Carlo simulations with AR (1) surrogates used to evaluate the significance levels of the maximum observed r^2envelope (A), r^2power (B), and r^2opt (C) for the Middle Member of the Dawenkou Formation at sedimentation rate of 16.71 cm/kyr.

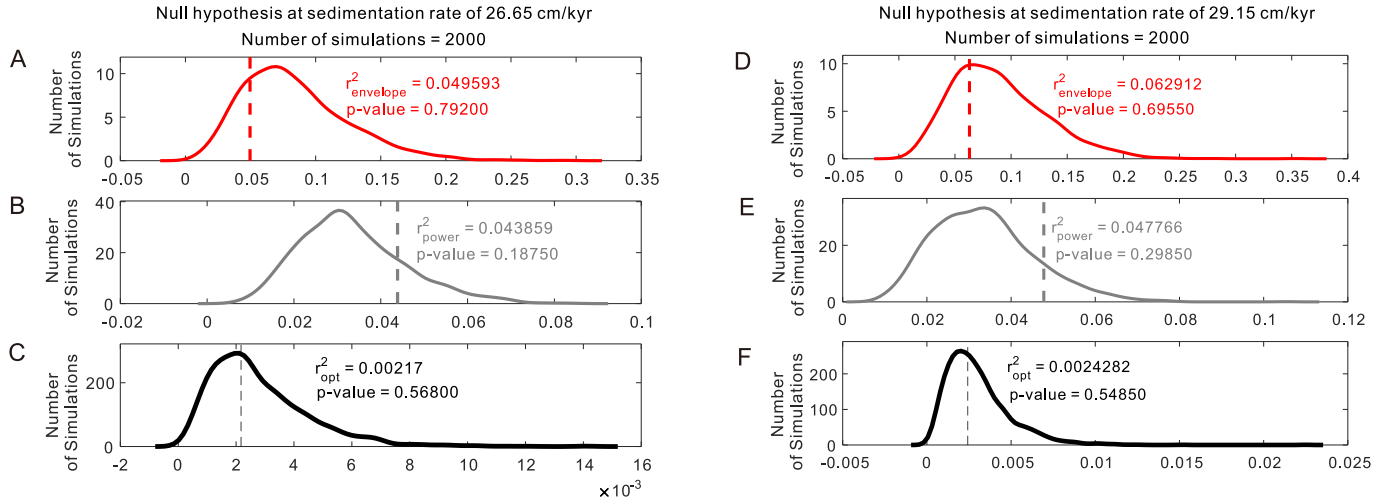

Fig. 9. Summary of 2000 Monte Carlo simulations with AR (1) surrogates used to evaluate the significance levels of the maximum observed r^2envelope (A, D), r^2power (B, E), and r^2opt (C, F) at sedimentation rate of 26.65 cm/kyr (A-C) and 29.15 cm/kyr (D-F).

BBB (Fig. 11). Based on the 405-kyr-tuned GR sequence, we calculate that the sedimentary duration of the Middle and Upper members of the Dawenkou Formation in the Huanggang Basin is 6.5 Myr ± 0.4 Myr (Section 4.3), which is within the total sedimentary duration of Es3 and Es2 (both span ~ 10.53 Myr according to Liu et al., 2018).

The Dongpu Depression, situated west of the Huanggang Basin, is one of the most important salt-bearing depressions in the BBB (Fig. 1B). Halites here are deposited mainly in four intervals, that is: the lower Es1, the first and second parts of Es3, the third part of Es3, and the fourth part of Es3 and the upper Es4 (Gao et al., 2015). Based on the time scales established by Liu et al. (2018) and Wang et al. (2020), we propose that halites of the Dawenkou Formation in the Huanggang Basin may have been deposited contemporaneously with the upper part of Es3 in the Dongpu Depression. The results from this study show that sedimentation of the salt-bearing Middle Member of the Dawenkou Formation lasted for about 4.05 Myr, which is shorter than the sedimentation period of the whole Es3 spanning about 6.48 Myr. Due to lack of drilling data from the Lower Member of the Dawenkou Formation and the underlying strata, it is unknown whether there is halite deposition in the deeper Huanggang Basin.

5.2. *Astronomical forcing of halite deposition*

Paleobotany and lithofacies studies reveal that the Huanggang Basin was in the arid /semi-arid climate zone, which runs through the east and west of China during the Paleogene (Sun and Wang, 2005). The generally dry climate provides a favorable environment for halite deposition. The halite-gypsum mudstone-mudstone rhythms in the Middle Member

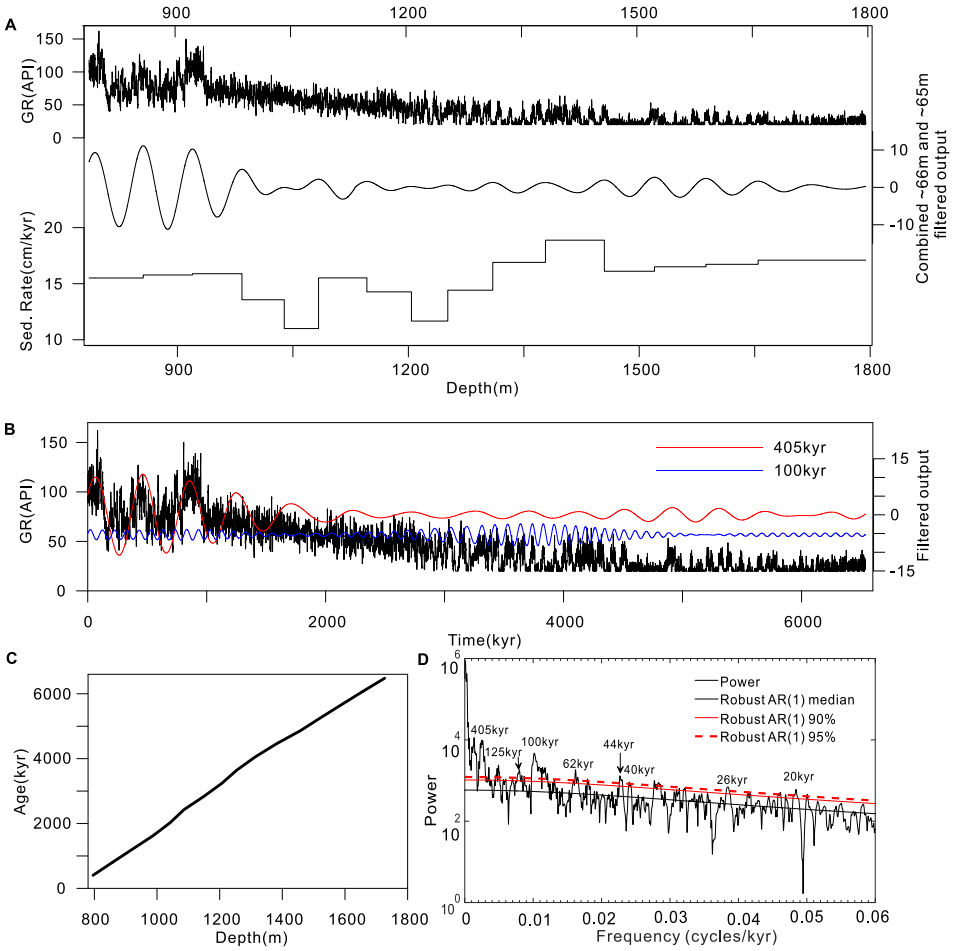

Fig. 10. (A) The original GR series, the combined ~ 66.0 m and ~ 65.0 m filtered output curve, and the sedimentation rate curve from top to bottom. (B) The 405-kyr-tuned GR series, the 405 kyr and 100 kyr filtered output curves (passband: 0.00247 ± 0.0003, 0.01 ± 0.0003). (C) The constructed age model. (D) The 2π MTM power spectrum of the tuned GR series.

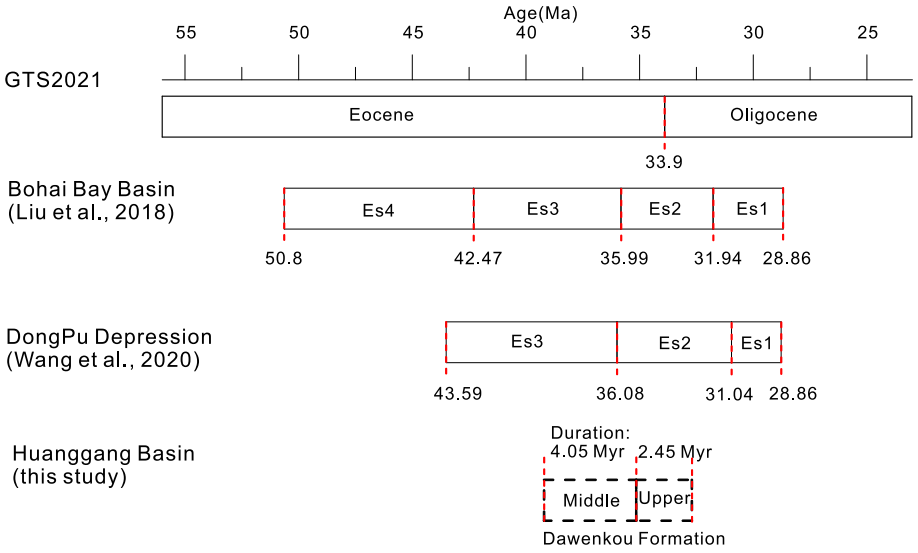

Fig. 11. Age comparisons among the Bohai Bay Basin, the Dongpu Depression, and the Huanggang Basin. Black dashed lines for the Huanggang Basin imply the likely depositional age of the Upper and Lower members of the Dawenkou Formation.

of the Dawenkou Formation reflects detailed dry-wet climatic cycles under a broadly arid regime. The sedimentary features and lithological changes observed in the Middle and Upper members of the Dawenkou Formation based on data from the ZK01 borehole reflect the evolution process of the lake from a semi-saline to a saline, and then to a fresh-water lake.

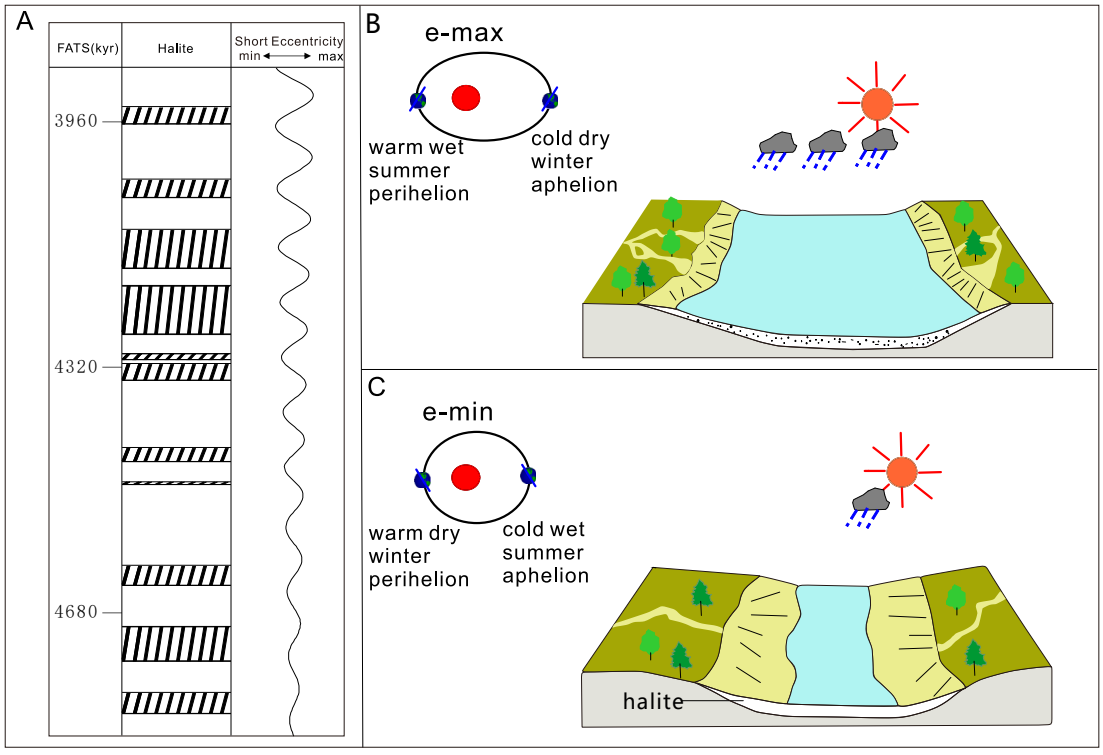

Fig. 12. A conceptual model for eccentricity-driven effect on climatic change on halite deposition during the Paleogene period.

Characterizing the geometric shape of the Earth's orbit, eccentricity itself does not provide significant insolation differences to modify climatic patterns but is a modulator of precession (Berger et al., 1992; Huybers and Aharonson, 2010). During eccentricity maxima, precession extremes can lead to insolation differences of about 20% (Laskar et al., 2004; Abels et al., 2013). The orbital precession affects the temporal distribution of the insolation between the winter and the summer. When the eccentricity is high, the shape of the Earth's orbit is an ellipse. The relative apparent climatic effect of precession leads to obvious seasonal contrasts. When the eccentricity is low, the Earth's orbit is close to a circle. The weak climatic effect of precession may only generate a subtle seasonal difference.

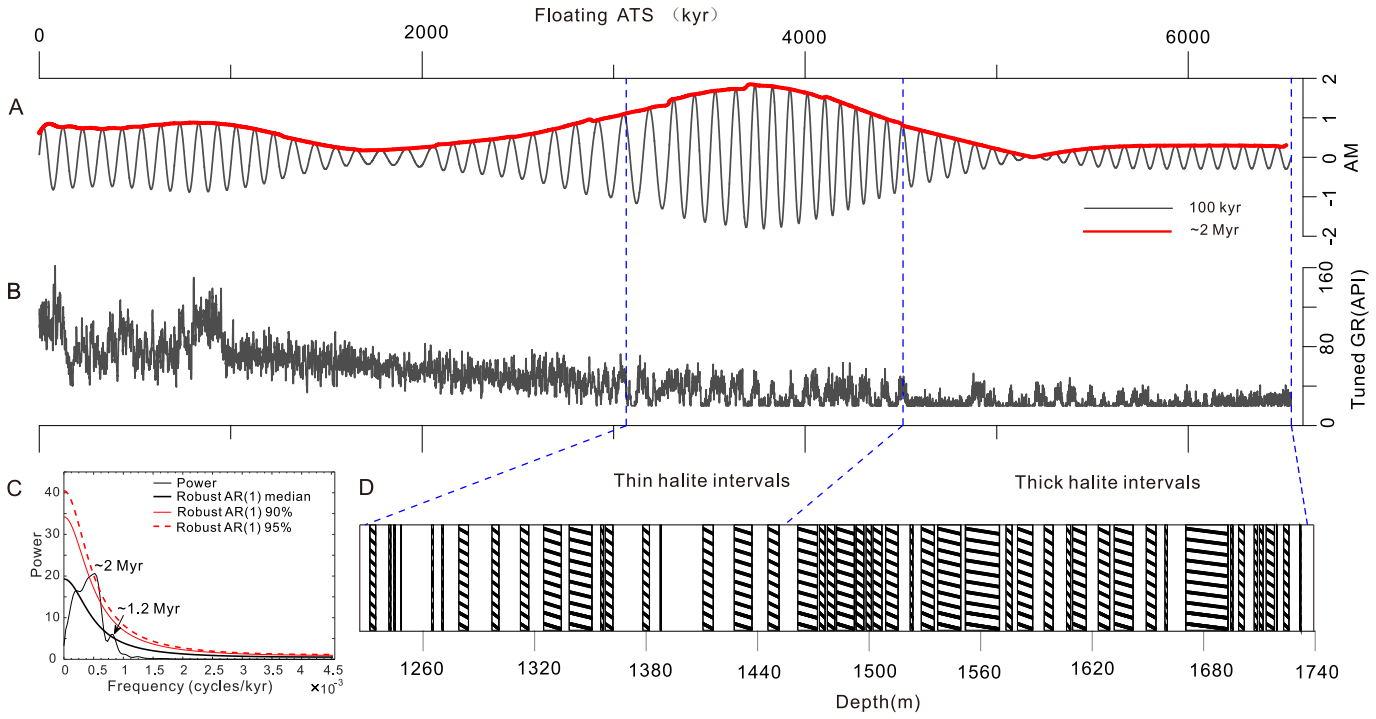

Fig. 13. Potential astronomical forcings on the halite formation in the Middle Member of the Dawenkou Formation, Huanggang Basin. (A) The 100 kyr filtered output curve (black) of the 405-kyr-tuned GR series (B) and its amplitude modulation (red). (C) The 2π MTM power spectrum of the AM, suggesting a ~ 2 Myr period with more than 95% confidence level. (D) The halite layers in the Middle Member of the Dawenkou Formation.

The gamma-ray intensity of radioactive elements (^{4}K, ^{232}Th, and ^{238}U) in sedimentary rocks can reflect variations in the clay mineral concentration in the sediments, which is indicative of the fluctuations of sea/lake levels and the input of terrestrial debris (Li et al., 2016a; Li et al., 2016b; Chen et al., 2020). During periods of high eccentricity, the hotter summers relative to colder winters produce an intensified monsoonal climate. Increased summer precipitation leads to a wetter climate, intense weathering (more clay production), more runoff, and the formation of deepening and broadening lakes, hence a high gamma-ray from the clay-rich intervals (Boulila et al., 2010; Li et al., 2016b; Li et al., 2017). During episodes of low eccentricity, cooler summers and warmer winters result in a weaker monsoonal and more semi-arid climate, thus leading to shallowing and shrinking of lakes (Boulila et al., 2010; Li et al., 2016b; Li et al., 2017) with salt-bearing minerals deposition in the saline lake system that would be characterized by low gamma-ray. Because halites are associated with relatively dry environments, halite occurrences in the sedimentary record would presumably reflect times of low orbital eccentricity and corresponding low gamma-ray record.

Despite the relatively few studies on the paleoclimatic forcings on halite formation cycles, nearly all of them suggest the significant forcing of 100 kyr short eccentricity on the deposition of halites (e.g., Williams, 1991; Huang and Hinnov, 2014, 2019). In this study, both the MTM spectrum and evolutionary wavelet analysis of the Middle Member of the Dawenkou Formation demonstrate a dominant ~ 16 m period signal corresponding to the 100 kyr astronomical period, which is well consistent with existing research.

The band-pass filtering of 100 kyr period in the Middle Member of the Dawenkou Formation indicates good correspondence with the halite interval and the minima of the short eccentricity (Fig. 12A). We suggest that the formation of halite may be influenced by seasonal variations, which is often controlled by orbital eccentricity. We propose a conceptual model to explore forcings of short eccentricity on halite deposition due to its influence on climate change. Low orbital eccentricity generally leads to low seasonality (Huang and Hinnov, 2019). When perihelion occurred in the Northern Hemisphere winter, winters were warm and dry while summers were relatively cool, leading to halite deposition (Fig. 12C). Orbital eccentricity maxima are always associated with high seasonal contrast. When perihelion occurred in the Northern Hemisphere summer, warm/wet summers and cold winters favored stronger monsoonal activity, increased run-off, and silt-mud deposition (Fig. 12B). Our conceptual model is similar to that of Huang and Hinnov (2019).

We note, however, that the thick halite intervals between 1450 and 1732 m do not strictly correspond to the minima of the short eccentricity. The amplitude modulation of the 100 kyr eccentricity period (Fig. 13A) and its spectral analysis result (Fig. 13C) suggest that the sedimentary record is also regulated by the ~ 2 Myr eccentricity period. During arid environment in general, a low amplitude of ~ 2 Myr eccentricity means relatively small seasonal differences during the deposition. Longer warm/dry winters and shorter cool/wet summers might be more favorable to the formation of thick halite layers. With the increase in the amplitude of the ~ 2 Myr eccentricity, the seasonality gradually increases, which leads to the development of thin halite layers due to the short eccentricity cycles.

6. Conclusions

During the middle and late Eocene to early Oligocene, a more than 1000-m-thick lacustrine succession with decimeter to decameter-scale halite-gypsum mudstone-mudstone rhythms were deposited as part of the Dawenkou Formation in the Huanggang Basin (Eastern China) and provides an ~ 6.5-Myr-long continuous sedimentary record of hot/dry to cool/wet continental climate cycles. The halite-gypsum mudstone-mudstone rhythms in the Middle Member of the Dawenkou Formation are paced by astronomical forcings. The dominant ~ 16 m cycles correspond to ~ 100 kyr orbital eccentricity, and halite deposits mostly occurred during periods of minimum short eccentricity.

During episodes of low short eccentricity when perihelion occurred in the Northern Hemisphere winter, warm/dry winters, and cool summers led to halite deposition. However, during periods of orbital eccentricity maximum when the summer of the Northern Hemisphere is close to the perihelion, hot/humid summers and cold/dry winters make strong seasonal differences, which lead to stronger monsoon activities, increased runoff, and silty-muddy depositions.

Under an arid climatic regime when the amplitude of super-long eccentricity is low, the seasonal differences in depositional processes are very small. Results from this study suggest that longer warm/dry winters and shorter cool/wet summers are more favorable to the formation of thick halite layers.

Declaration of Competing Interest

The authors declare that they have no known competing financial interests or personal relationships that could have appeared to influence the work reported in this paper.

Data availability

Data will be made available on request.

Acknowledgments

This study was financially supported by National Key Research and Development Program of China (Grant No. 2022YFC2903402), the SDUST (Shandong University of Science and Technology) Research Fund (Grant No. 2018TDJH101), and the SDUST Domestic Visiting Scholar Program. We thank the editors and two anonymous reviewers for their constructive comments.

Appendix A. Supplementary data

Supplementary data to this article can be found online at https://doi.org/10.1016/j.oregeorev.2023.105506.

References

Abels, H.A., Dupont-Nivet, G., Xiao, G., Bosboom, R., Krijgsman, W., 2011. Step-wise change of Asian interior climate preceding the Eocene-Oligocene Transition (EOT). Palaeogeogr. Palaeoclimatol. Palaeoecol. 299, 399–412.

Abels, H.A., Kraus, M.J., Gingerich, P.D., Sheldon, N., 2013. Precession-scale cyclicity in the fluvial lower Eocene Willwood Formation of the Bighorn Basin, Wyoming (USA). Sedimentology 60, 1467–1483.

Anderson, R.Y., 2011. Enhanced climate variability in the tropics: a 200 000 yr annual record of monsoon variability from Pangea's equator. Clim. Past 7, 757–770.

Berger, A., Loutre, M.-F., Laskar, J., 1992. Stability of the astronomical frequencies over the Earth's history for paleoclimate studies. Science 255, 560–566.

Boulila, S., Galbrun, B., Hinnov, L.A., Collin, P.Y., Ogg, J.G., Fortwengler, D., Marchand, D., 2010. Milankovitch and sub-Milankovitch forcing of the Oxfordian (Late Jurassic) Terres Noires Formation (SE France) and global implications. Basin Res. 22, 717–732.

Boulila, S., Vahlenkamp, M., De Vleeschouwer, D., Laskar, J., Yamamoto, Y., Pälike, H., Kirtland Turner, S., Sexton, P.F., Westerhold, T., Röhl, U., 2018. Towards a robust and consistent middle Eocene astronomical timescale. Earth Planet. Sci. Lett. 486, 94–107.

Chen, G., Gang, W., Tang, H., Gao, G., Wang, N., Liu, L., Yang, S., Wang, Y., 2020. Astronomical cycles and variations in sediment accumulation rate of the terrestrial lower Cretaceous Xiagou Formation from the Jiuquan Basin, NW China. Cretac. Res. 109, 104156. https://doi.org/10.1016/jcretres. 2019. 06.002.

De Vleeschouwer, D., Da Silva, A.C., Sinnesael, M., Chen, D., Day, J.E., Whalen, M.T., Guo, Z., Claeys, P., 2017. Timing and pacing of the Late Devonian mass extinction event regulated by eccentricity and obliquity. Nat. Commun. 8, 2268. https://doi.org/10.1038/s41467-017-02407-1.

Du, W., Ji, Y., Chen, G., Wu, H., Gao, C., Li, S., Zhang, Y., 2020. Cyclostratigraphy and astronomical tuning during the Oligocene in the Jizhong Depression, Bohai Bay Basin, northeastern China. Palaeogeogr. Palaeoclimatol. Palaeoecol. 554, 109803. https://doi.org/10.1016/j. palaeo.2020.109803.

Eldrett, J.S., Ma, C., Bergman, S.C., Lutz, B., Gregory, F.J., Dodsworth, P., Phipps, M., Hardas, P., Minisini, D., Ozkan, A., Ramezani, J., Bowring, S.A., Kamo, S.L.,

Ferguson, K., Macaulay, C., Kelly, A.E., 2015a. An astronomically calibrated stratigraphy of the Cenomanian, Turonian and earliest Coniacian from the Cretaceous Western Interior Seaway, USA: implications for global chronostratigraphy. Cretac. Res. 56, 316–344.
Eldrett, J.S., Ma, C., Bergman, S.C., Ozkan, A., Minisini, D., Lutz, B., Jackett, S.-J., Macaulay, C., Kelly, A.E., 2015b. Origin of limestone–marlstone cycles: Astronomic forcing of organic-rich sedimentary rocks from the Cenomanian to early Coniacian of the Cretaceous Western Interior Seaway, USA. Earth Planet. Sci. Lett. 423, 98–113.
Filippi, M., Bruthans, J., Palatinus, L., Zare, M., 2011. Secondary halite deposits in the Iranian salt karst: general description and origin. Int. J. Speleol. 40 (2), 141–162.
Gao, H., Zheng, R., Xiao, Y., Meng, F., Chen, F., Bai, G., Luan, Y., Tan, X., Shi, Y.e., 2015. Origin of the salt rock of Palegene Shahejie Formation of Dongpu Sag, Bohai Bay Basin: evidence from sedimentology and geochemistry. Acta Pet. Sin. 36, 19–32.
Hinnov, L.A., 2013. Cyclostratigraphy and its revolutionizing applications in the earth and planetary sciences. Geol. Soc. Am. Bull. 125, 1703–1734.
Hollaar, T.P., Baker, S.J., Hesselbo, S.P., Deconinck, J.-F., Mander, L., Ruhl, M., Belcher, C.M., 2021. Wildfire activity enhanced during phases of maximum orbital eccentricity and precessional forcing in the Early Jurassic. Commun. Earth Environ. 2, 247. https://doi.org/10.1038/s43247-021-00307-3.
Huang, C., Hinnov, L., 2014. Evolution of an Eocene-Oligocene saline lake depositional system and its controlling factors, Jianghan Basin, China. J. Earth Sci. 25, 959–976.
Huang, C., Hinnov, L., 2019. Astronomically forced climate evolution in a saline lake record of the middle Eocene to Oligocene, Jianghan Basin, China. Earth Planet. Sci. Lett. 528, 115846. https://doi.org/10.1016/j.epsl.2019.115846.
Huybers, P., Aharonson, O., 2010. Orbital tuning, eccentricity, and the frequency modulation of climatic precession. Paleoceanography 25. https://doi.org/10.1029/2010PA001952.
Kemp, D.B., Coe, A.L., Cohen, A.S., Weedon, G.P., 2011. Astronomical forcing and chronology of the early Toarcian (Early Jurassic) oceanic anoxic event in Yorkshire, UK. Paleoceanography 26. https://doi.org/10.1029/2011PA002122.
Laskar, J., Robutel, P., Joutel, F., Gastineau, M., Correia, A., Levrard, B., 2004. A long-term numerical solution for the insolation quantities of the Earth. Astron. Astrophy. 428, 261–285.
Lei, C., 1984. Early Tertiary spores and pollen grains from Dawenkou Formation of Shandong and its stratigraphic significance. J. East China Petrol. Inst. 42–55.
Lepre, C.J., Quinn, R.L., 2022. Aridification and orbital forcing of eastern African climate during the Plio-Pleistocene. Global Planet. Change 208, 103684. https://doi.org/10.1016/j.gloplacha.2021. 103684.
Li, M., Barnes, H.L., 2019. Orbitally forced sphalerite growth in the Upper Mississippi Valley District. Geochem. Perspecti. Lett. 18–22.
Li, Y., Gill, B., Montañez, I.P., Ma, L., LeRoy, M., Kodama, K.P., 2020b. Orbitally driven redox fluctuations during Cretaceous Oceanic Anoxic Event 2 (OAE2) revealed by a new magnetic proxy. Palaeogeogr. Palaeoclimatol. Palaeoecol. 538, 109465. https://doi.org/10.1016/j.palaeo. 2019.109465.
Li, M., Huang, C., Hinnov, L., Ogg, J., Chen, Z.-Q., Zhang, Y., 2016a. Obliquity-forced climate during the Early Triassic hothouse in China. Geology 44, 623–626.
Li, M., Ogg, J., Zhang, Y., Huang, C., Hinnov, L., Chen, Z.-Q., Zou, Z., 2016b. Astronomical tuning of the end-Permian extinction and the Early Triassic Epoch of South China and Germany. Earth Planet. Sci. Lett. 441, 10–25.
Li, M., Zhang, Y., Huang, C., Ogg, J., Hinnov, L., Wang, Y., Zou, Z., Li, L., 2017. Astronomical tuning and magnetostratigraphy of the Upper Triassic Xujiahe Formation of South China and Newark Supergroup of North America: Implications for the Late Triassic time scale. Earth Planet. Sci. Lett. 475, 207–223.
Li, M., Kump, L.R., Hinnov, L.A., Mann, M.E., 2018. Tracking variable sedimentation rates and astronomical forcing in Phanerozoic paleoclimate proxy series with evolutionary correlation coefficients and hypothesis testing. Earth Planet. Sci. Lett. 501, 165–179.
Li, M., Hinnov, L., Kump, L., 2019. Acycle: Time-series analysis software for paleoclimate research and education. Comput. Geosci. 127, 12–22.
Li, M., Sun, S., Yan, M., Meng, F., Fang, X., Song, X., Zhu, L., 2020a. Late Cretaceous paleoclimate reconstruction from halite in an evaporite deposit on the Khorat Plateau, Laos. Cretac. Res. https://doi.org/10.1016/j.cretres.2020.104589.
Liu, Q., Chen, Y., Li, Y., Lan, Q., Yuan, H., Yan, D., 1987. Mesozoic and Cenozoic terrigenous clastic chemical rock type salt deposits in China. Beijing Science and Technology Press, Beijing.
Liu, Z., Huang, C., Algeo, T.J., Liu, H., Hao, Y., Du, X., Lu, Y., Chen, P., Guo, L., Peng, L., 2018. High-resolution astrochronological record for the Paleocene-Oligocene (66–23 Ma) from the rapidly subsiding Bohai Bay Basin, northeastern China. Palaeogeogr. Palaeoclimatol. Palaeoecol. 510, 78–92.
Lu, S., Yang, B., Li, S., Song, X., Du, S., Gao, J., Zhang, S., Li, M., Zhang, W., 2021. Paleogene Environmental Changes Recorded by the Borehole in the Shanxian Basin, Southwestern Shandong. Acta Sedimentol. Sin. 10.14027/j.issn.1000-0550.2021.090.
Lv, D., Wang, L., Isbell, J.L., Lu, C., Li, P., Wang, Y., Zhang, Z., 2022. Records of chemical weathering and volcanism linked to paleoclimate transition during the Late Paleozoic Icehouse. Global Planet. Change 217, 103934. https://doi.org/10.1016/j.gloplacha.2022.103934.
Meyers, S.R., 2015. The evaluation of eccentricity-related amplitude modulation and bundling in paleoclimate data: An inverse approach for astrochronologic testing and time scale optimization. Paleoceanography 30, 1625–1640.
Scotese, C.R., Wright, N., 2018. PALEOMAP Paleodigital Elevation Models (Paleo-DEMS) for the Phanerozoic PALEOMAP Project, https://www.earthbyte .org /paleodem -resource -scotese -and -wright -2018/.
Shi, J., Jin, Z., Liu, Q., Huang, Z., Hao, Y., 2018. Terrestrial sedimentary responses to astronomically forced climate changes during the Early Paleogene in the Bohai Bay Basin, eastern China. Palaeogeogr. Palaeoclimatol. Palaeoecol. 502, 1–12.
Shi, J., Jin, Z., Liu, Q., Zhang, R., Huang, Z., 2019. Cyclostratigraphy and astronomical tuning of the middle eocene terrestrial successions in the Bohai Bay Basin, Eastern China. Global Planet. Change 174, 115–126.
Shi, J., Jin, Z., Liu, Q., Huang, Z., 2020. Depositional process and astronomical forcing model of lacustrine fine-grained sedimentary rocks: a case study of the early Paleogene in the Dongying Sag, Bohai Bay Basin. Mar. Pet. Geol. 113, 103995. https://doi.org/10.1016/j.marpetgeo.2019.08.023.
Shi, J., Jin, Z., Liu, Q., Fan, T., Gao, Z., 2021. Sunspot cycles recorded in Eocene lacustrine fine-grained sedimentary rocks in the Bohai Bay Basin, eastern China. Global Planet. Change 205, 103614. https://doi.org/10.1016/j.gloplacha.2021.103614.
Sinnesael, M., McLaughlin, P.I., Desrochers, A., Mauviel, A., Weirdt, J.D., Claeys, P., Vandenbroucke, T.R.A., 2021. Precession-driven climate cycles and time scale prior to the Hirnantian glacial maximum. Geology 49, 1295–1300.
Smykatz-Kloss, W., Roy, P.D., 2010. Evaporite mineralogy and major element geochemistry as tools for palaeoclimatic investigations in arid regions: a synthesis. Bol. Soc. Geol. Mex. 62 (3), 379–390.
Sonnenfeld, P., 1984. Brines and Evaporites. Academic Press, New York.
Sun, X., Wang, P., 2005. How old is the Asian monsoon system?—Palaeobotanical records from China. Palaeogeogr. Palaeoclimatol. Palaeoecol. 222, 181–222.
Tang, L., Zhang, S., Yu, X., Tian, J., Yang, B., Luo, W., Chen, W., Liang, J., Ma, X., Wu, K., 2021. Geological characteristics and prospecting potentials of rock salt deposit in Huanggang Subdepression in southwest Shandong Province. Shandong Land Resour. 37, 1–10.
Wang, M., Chen, H., Huang, C., Kemp, D.B., Xu, T., Zhang, H., Li, M., 2020. Astronomical forcing and sedimentary noise modeling of lake-level changes in the Paleogene Dongpu Depression of North China. Earth Planet. Sci. Lett. 535, 116116. https://doi.org/10.1016/j. marpetgeo.2019.08.023.
Wang, L., Lv, D., Hower, J.C., Zhang, Z., Raji, M., Tang, J., Liu, Y., Gao, J., 2022. Geochemical characteristics and paleoclimate implication of Middle Jurassic coal in the Ordos Basin, China. Ore Geol. Rev. 144, 104848. https://doi.org/10.1016/j.oregeorev.2022.104848.
Williams, G.E., 1991. Milankovitch-band cyclicity in bedded halite deposits contemporaneous with Late Ordovician-Early Silurian glaciation, Canning Basin, Western Australia. Earth Planet. Sci. Lett. 103, 143–155.
Worley, N.E., 2005. The occurrence of halite in the Permian A Bed Evaporite, Kirkby Thore, Cumbria. Proc. Yorks. Geol. Soc. 55 (3), 199–203.
Wu, H., Zhang, S., Hinnov, L.A., Jiang, G., Feng, Q., Li, H., Yang, T., 2013. Time-calibrated Milankovitch cycles for the late Permian. Nat. Commun. 4, 2452. https://doi.org/10.1038/ncomms3452.
Wu, H., Hinnov, L.A., Zhang, S., Jiang, G., Yang, T., Li, H., Xi, D., Ma, X., Wang, C., 2022. Continental geological evidence for Solar System chaotic behavior in the Late Cretaceous. GSA Bull. https://doi.org/10.1130/B36340.1.
Xiao, G., Abels, H.A., Yao, Z., Dupont-Nivet, G., Hilgen, F.J., 2010. Asian aridification linked to the first step of the Eocene-Oligocene Climate Transition (EOT) in obliquity-dominated terrestrial records in Xining Basin, China. J. Earth Sci. 6, 627–657.
Yao, X., Zhou, Y., Hinnov, L.A., 2015. Astronomical forcing of a Middle Permian chert sequence in Chaohu, South China. Earth Planet. Sci. Lett. 422, 206–221.
Zhang, Z., Lv, D., Wang, T., An, D., Liu, H., Wang, D., Wang, C., 2022. Intensive peatland wildfires during the Aptian-Albian oceanic anoxic event 1b: Evidence from borehole SK-2 in the Songliao Basin, NE China. J. Palaeogeogr. 11 (3), 448–467.
Zhang, J., Pas, D., Krijgsman, W., Wei, W., Du, X., Zhang, C., Liu, J., Lu, Y., 2020a. Astronomical forcing of the Paleogene coal-bearing hydrocarbon source rocks of the East China Sea Shelf Basin. Sed. Geol. https://doi.org/10.1016/j.sedgeo.2020.105715.
Zhang, S., Wang, X., Hammarlund, E.U., Wang, H., Costa, M.M., Bjerrum, C.J., Connelly, J.N., Zhang, B., Bian, L., Canfield, D.E., 2015. Orbital forcing of climate 1.4 billion years ago. PNAS 112, E1406–E1413.
Zhang, Z., Wang, C., Lv, D., Hay, W.W., Wang, T., Cao, S., 2020c. Precession-scale climate forcing of peatland wildfires during the early middle Jurassic greenhouse period. Global Planet. Change 184, 103051. https://doi.org/10.1016/j.gloplacha.2019.103051.
Zhang, T., Zhang, C., Fan, T., Zhang, L., Zhu, R., Tao, J., Li, M., 2020b. Cyclostratigraphy of Lower Triassic terrestrial successions in the Junggar Basin, northwestern China. Palaeogeogr. Palaeoclimatol. Palaeoecol. 539, 109493. https://doi.org/10.1016/j.palaeo.2019.109493.